



## Simple route synthesis of $\text{MnFe}_2\text{O}_4$ @ alunite composite for preconcentration of trace level of copper and lead from food and water samples

Mahsa Shirkhodaie, Mostafa Hossein Beyki, Farzaneh Shemirani\*

*School of Chemistry, University College of Science, University of Tehran, P.O. Box 14155-6455, Tehran, Iran, Tel. +98 21 61112481; Fax: +98 21 66405141; emails: hosseinbakim@gmail.com (M. Hossein Beyki), Shemiran@khayam.ut.ac.ir (F. Shemirani), m.shirkhodaie@gmail.com (M. Shirkhodaie)*

Received 26 June 2015; Accepted 4 December 2015

### ABSTRACT

A novel magnetic alunite@ $\text{MnFe}_2\text{O}_4$  nanocomposite has been synthesized by one-step refluxing coprecipitation method. XRD, SEM, VSM, and FT-IR techniques were carried out to characterize calcined alunite as well as the prepared nanocomposite. The synthetic process is facial, simple, and fast. Moreover, as-synthesized nanocomposite bears compelling features including superparamagnetic property, chemical stability, and high adsorption capacity, which makes it apt for preconcentration and separation of trace amounts of Cu(II) and Pb(II) ions from different samples. Optimal experimental conditions such as pH, adsorbent dosage, and contact time have been established. At the optimum pH of 6–7, metal ions were quantitatively sorbed onto the proposed adsorbent then desorbed with 5 mL of  $0.5 \text{ mol L}^{-1} \text{ HNO}_3$ . The detection limit of Cu(II) and Pb(II) was  $0.91$  and  $0.69 \text{ } \mu\text{g L}^{-1}$ , respectively. Linearity was maintained at  $0.004$ – $0.150 \text{ mg L}^{-1}$  for copper and at  $0.005$ – $0.150 \text{ mg L}^{-1}$  for lead ions. The experimental data were analyzed by the Langmuir and Freundlich adsorption models. Both models provided the best correlation of the experimental data and the maximum capacity was found to be  $129.87$  and  $158.78 \text{ mg g}^{-1}$  for copper and lead, respectively. The kinetic models have also been studied and results showed that the second-order model can describe the adsorption process.

*Keywords:* Manganese ferrite; Alunite; Magnetic composite; Solid-phase extraction

### 1. Introduction

The potassium alunite  $[\text{KAl}_3(\text{SO}_4)_2(\text{OH})_6]$ , which forms by hydrothermal alteration of volcanic rock in rhombohedral and hexagonal crystal, is one of the common member of alunites group. It is the mineral which can function as a commercial raw material for the chemical industry and has been widely used in manufacturing of aluminum sulfate, potassium alum,

alumina, and potassium sulfate. Moreover, it has also been used as an inorganic adsorbent for the removal of pollutants as it is enriched with the oxides of aluminum and silica [1,2]. Calcination of alunite at  $650$ – $900^\circ\text{C}$  produces  $\text{Al}_2\text{O}_3$  and  $\text{KAl}(\text{SO}_4)_2$  (alum) with excessive adsorption sites. Hence, it could be an appropriate choice as a sorbent in solid-phase extraction (SPE). There are only limited numbers of studies on alunite applicability in the removing of pollutants. Some reports include its employment as an adsorbent

\*Corresponding author.

for the removal of phosphate, boron, and dyes [3,4]. However, there are no reports on the preconcentration and removal of heavy metals using alunite as an adsorbent.

Common solid adsorbents have been applied in column or batch procedure. The conventional adsorption procedures usually beget poor recovery of the target analytes and a long equilibrium time of SPE when it deals with large sample volume owing to the limited rate of diffusion and mass transfer. Furthermore, in the batch procedure, collection of adsorbent from sample solution requires centrifugation, or filtration, which could be difficult and time-consuming [5–7]. In order to overcome these limitations, there has been an increasing interest in the use of magnetic nanocomposites as adsorbents in SPE. Magnetic nanoparticles bring about sufficient large contact area between the adsorbent and analytes [8,9]. Therefore, rapid mass transfer can be obtained, which leads to shorter extraction time, much greater extraction capacity, and reduction in the amount of required sorbent. Furthermore, magnetic separation could be applied as an easy, effective, and quick method for the collection of solid adsorbent from the solution [10,11]. Recently, several types of magnetic nanoparticles have been used as an adsorbent in several kinds of remediation techniques. One of these magnetic nanoparticles is group of ferrite nanoparticles which could be used in various areas. Manganese ferrite ( $\text{MnFe}_2\text{O}_4$ ) is a kind of spinel ferrite which has an excellent properties such as high saturation magnetization, initial permeability, and resistivity, as well as low losses compared to other ferrites, and also its magnetic property is higher than of other ferrite nanoparticles [12,13]. The preparation techniques of manganese ferrite nanoparticles have been performed via various methods such as ball milling, sol-gel, hydrothermal, and chemical coprecipitation techniques. In view of simplicity, low cost, and short preparation time, the latter is preferred [14–16]. Recently, combination of magnetic nanoparticles and non-magnetic adsorbent by taking advantage of both has gained much interest. However, the common synthetic routes of magnetic nanocomposite are tedious and time-consuming. For this reason, one-step preparation of magnetic nanoparticles and simultaneously bonding to the template give rise to great interests [17,18].

Determination of trace amounts of heavy metals such as copper and lead has always been in attention. Despite the fact that among the heavy metals copper is an essential element for all living organisms at the very trace amounts, it could be toxic and hazardous like lead in excessive amounts in as much as both of them are non-biodegradable and have persistent nature [19]. They could contaminate the environment,

accumulate in living tissues, and consequently give rise to various fatal diseases. In other words, they could be a serious threat to ecological system and human beings. Hence, their enrichment and determination at trace levels is of great importance [20].

To the best of our knowledge, there is no report neither on the preparation of  $\text{MnFe}_2\text{O}_4$ @alunite nanocomposite nor on its application for magnetic SPE of heavy metals. In this study,  $\text{MnFe}_2\text{O}_4$ @alunite nanocomposite was synthesized by very facile refluxing coprecipitation method for the first time. The potential of as-synthesized  $\text{MnFe}_2\text{O}_4$ @alunite nanocomposite for SPE of copper and lead was investigated. In fact, we used a magnetic mixed oxide as a solid sorbent for heavy metal preconcentration. The sorbent contains  $\text{Al}_2\text{O}_3$ ,  $\text{Fe}_2\text{O}_3$ , and  $\text{MnO}$  as the main fragments. The first oxide, alumina, was obtained from a natural source as a result of a simple calcination route. In other words, the substrate can be easily accessible and has low cost which made the final composite cost-effective. Moreover, preparation of the magnetic composite is simple and fast, as well as magnetic characteristic of the sorbent made the extraction procedure more efficient. Especially, the synthetic route can be performed with anyone and the sorbent can be manipulated from reaction vessel by simple external magnetic field. The SPE conditions, including pH, amount of solvents, equilibrium time, and desorption conditions, were optimized. In addition, the experimental data were correlated to different kinetic and adsorption isotherm models and corresponding parameters were determined.

## 2. Experimental

### 2.1. Reagents and solutions

$\text{Fe}(\text{NO}_3)_3 \cdot 9\text{H}_2\text{O}$ ,  $\text{Mn}(\text{NO}_3)_2 \cdot 4\text{H}_2\text{O}$ ,  $\text{KCl}$ , and  $\text{NaOH}$  were analytical grade and supplied from Merck (Merck, Darmstadt, Germany). Standard solutions of heavy metals ( $1,000 \text{ mg L}^{-1}$ ) were prepared by dissolving proper amounts of nitrate salts in distilled water. More dilute solutions were prepared daily from  $1,000 \text{ mg L}^{-1}$  stock solutions. The pH adjustment was done by the addition of dilute hydrochloric acid or ammonia to prepare the desired pH solution. All acids and bases were used in their analytical grade. Plastic and glassware were cleaned by soaking in diluted  $\text{HNO}_3$  or  $\text{HCl}$  and rinsed with distilled water prior to their use.

### 2.2. Instruments

A Varian model AA-400 flame atomic absorption spectrometer (FAAS, Varian Australia Pty Ltd,

Musgrave), equipped with a deuterium lamp background, hollow cathode lamps, and air-acetylene flame, was used for analysis. All instrumental settings were those of recommended by the manufacturer. The digital pH meter model 781 from Metrohm (Herisau, Switzerland) equipped with glass-combined electrode was used for the pH adjustments. The prepared particles were characterized by powder X-ray diffraction analysis using a Phillips powder diffractometer, X'Pert MPD, with Cu-K $\alpha$  ( $\lambda = 1.540589 \text{ \AA}$ ) radiation. Surface morphology analysis of the magnetic composite was carried out using HITACHI S 4160. Fourier transform infrared spectra (FT-IR) were measured with ATR method by Equinox 55 Bruker over the wavelength of 400–4,000  $\text{cm}^{-1}$ . Separation was assisted using a neodymium-iron-boron ( $\text{Nd}_2\text{Fe}_{12}\text{B}$ ) magnet.

### 2.3. Preparation of magnetic $\text{MnFe}_2\text{O}_4$ @calcined alunite nanocomposite

Ten grams of finely ground raw alunite was calcined in a furnace at the temperature of 700 °C for 1 h. Then, the calcined alunite was sieved through a 150-sieve and stored for further use. The  $\text{MnFe}_2\text{O}_4$ @alunite was synthesized through refluxing route. About 3.9 g iron nitrate and 1.2 g manganese nitrate were added to the mixture of 1.0 g alunite and 100 mL distilled water. The mixture was magnetically stirred for 15 min, then solution of 4 mol  $\text{L}^{-1}$  NaOH was added into the mixture under drastic stirring and the synthesis was carried out by magnetic stirring for 30 min at 90 °C. The obtained product was separated magnetically and washed several times with distilled water, then dried in the oven at 70 °C.

### 2.4. Metal adsorption characteristics of adsorbent

In order to investigate metal adsorption characteristics of manganese ferrite@calcined alunite, about 30 mg of sorbent was added to a series of 50 mL sample solutions of metal ions with the concentration of 5.0 mg  $\text{L}^{-1}$ . The pH of sample mixture was adjusted to about 6.0 using diluted solutions of HCl and  $\text{NH}_3$ . It was shaken for 10 min to reach the equilibrium. Then, the adsorbent was separated magnetically and residual metal concentrations in the supernatant were directly determined by FAAS. The results are depicted in Fig. 1(a). It can be seen that adsorption removal for Cd, Cu, and Pb was large enough. These three ions were effectively adsorbed onto the adsorbent. However, the recovery of cadmium ions were not quantitative. Thus, the nanocomposite could be used as a relatively selective sorbent toward both  $\text{Cu}^{2+}$  and  $\text{Pb}^{2+}$  in SPE.

### 2.5. Preconcentration procedure

For the preconcentration of Pb(II) and Cu(II), the procedure was carried out in a batch process. An optimum amount of magnetic  $\text{MnFe}_2\text{O}_4$ @calcined alunite nanocomposite (30 mg) was added to a series of 50 mL sample solutions containing aliquots of Pb(II) and Cu(II) ions in the range of 0.5–10  $\mu\text{g}$  as adsorbates. The pH of sample mixture was adjusted to optimum (6–7). After shaking for 10 min, the adsorbent was separated magnetically. Then, adsorbed analytes were eluted with 5 mL of 0.5 mol  $\text{L}^{-1}$   $\text{HNO}_3$  by shaking for 5 min and the analytes in the eluate were measured by FAAS. Blank solutions were also run under the same analytical conditions without adding analytes.

### 2.6. Preparation of water and digested real samples

To prepare water sample, 50 ml of sea water (Caspian sea) was filtered to remove any suspended particles and analyzed by described method. Acid-digested samples were prepared as follows: amounts of 50 mg of mushroom, tomato, and sausage were heated separately at 80 °C in an oven for 1 h. After cooling, each of the samples was digested with 10 ml of 3:1 HCl/ $\text{HNO}_3$  by heating at 90 °C until brown fumes ceased to evolve. Then, 10 ml of 30%  $\text{H}_2\text{O}_2$  solution was added to them and the solutions were heated until they became clear. After cooling the solutions to the room temperature, they were filtered and diluted with distilled water up to 100 ml. Then, pH adjustment was done and 50 ml of each sample was analyzed separately according to the proposed method under optimum conditions. Moreover, accuracy of the method was evaluated by spiking different amounts of Cu(II) and Pb(II) in 50 ml of samples.

## 3. Results and discussion

### 3.1. Characterization of Alunite@Manganese ferrite

The FT-IR spectra of raw alunite, calcined alunite, and alunite@manganese ferrite are shown in Fig. 1(b). In the spectrum of raw alunite, the peaks are at 3,100  $\text{cm}^{-1}$  related to hydroxyl ( $-\text{OH}$ ) stretching groups, which are not existed in calcined alunite spectrum. The bands at 1,100–1257  $\text{cm}^{-1}$ , as well as 1,217 and 1,085  $\text{cm}^{-1}$  are assigned to Al–O–M vibration (M=Si, Al) and the existence of S=O group, respectively. The appearance of new bands at 444, 504, and 542  $\text{cm}^{-1}$  can be attributed to Mn–O and Fe–O, indicating the successful preparation of  $\text{MnFe}_2\text{O}_4$  on the matrix of alunite.

Fig. 1(c) shows XRD patterns of calcined alunite and  $\text{MnFe}_2\text{O}_4$ @alunite. According to this pattern,

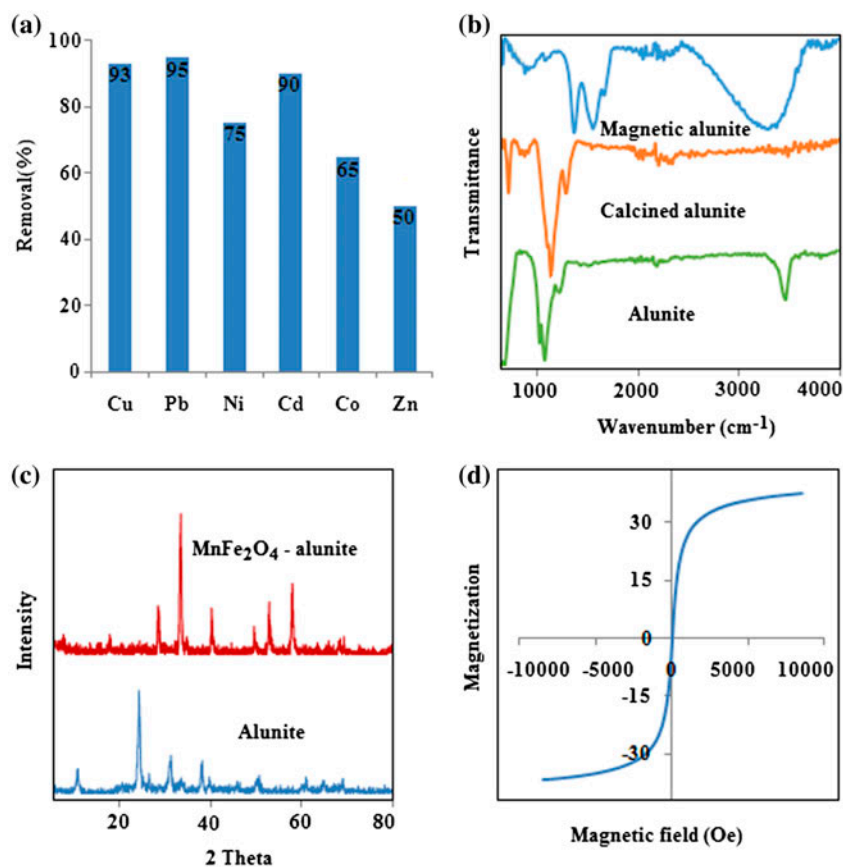


Fig. 1. Metal adsorption characteristic (a), the FT-IR spectra (b), the XRD pattern (c), and VSM graph (d) of the materials.

diffraction peaks for both spectra are well matched with the standard spectra of alunite (JCPDS no. 01-074-0082) and  $\text{MnFe}_2\text{O}_4$  (JCPDS no. 01-074-2403). The magnetic hysteresis loops of prepared composite are shown in Fig. 1(d). The saturated magnetization of the prepared composite was 36.0 emu/g. Furthermore, the remanence value is 0.27 emu/g which indicates that the magnetic composites are superparamagnetic nanoparticles with a single magnetic domain. To investigate the surface morphology of the synthesized alunite@manganese ferrite nanocomposite, the samples were characterized by SEM analysis (Fig. 2(a) and (b)). The image of magnetic alunite indicates more heterogeneous distribution of particle size than particle size of calcined alunite and the presence of some pores in its structure. The average diameter of  $\text{MnFe}_2\text{O}_4$ @alunite particles in nanocomposite which estimated from the SEM micrograph was approximately 45 nm.

### 3.2. Effect of pH

The pH of the solution is one of the crucial analytical factors in SPE, since the adsorption of heavy

metals from aqueous solutions is dependent on the pH of the solution which affects the surface charge of adsorbent, degree of ionization, and speciation of the adsorbate species [21,22]. In order to investigate the influence of this parameter on the adsorption of Cu(II) and Pb(II), as well as to determine the optimal pH, constant amount of adsorbent (30 mg) was suspended in 50 mL of Cu(II) and Pb(II) at the fixed concentration ( $5 \text{ mg L}^{-1}$ ) individually. The pH of both samples was adjusted to 1–10. Then, they were shaken for 10 min and adsorbent was magnetically separated. The amount of target ions was measured by FAAS and  $Q_e$ , the equilibrium adsorption capacity of adsorbent, was calculated with the Eq. (1):

$$Q_e = (C_i - C_e)V/m \quad (1)$$

where  $C_i$  and  $C_e$  ( $\text{mg L}^{-1}$ ) are initial and equilibrium liquid-phase concentrations of target ion, respectively.  $V$  is the volume of the solution (L) and  $m$  is the weight (g) of the adsorbent. As it was indicated in results (Fig. 3(a)), adsorption capacity of both Cu(II) and Pb(II) was increased with increasing pH and

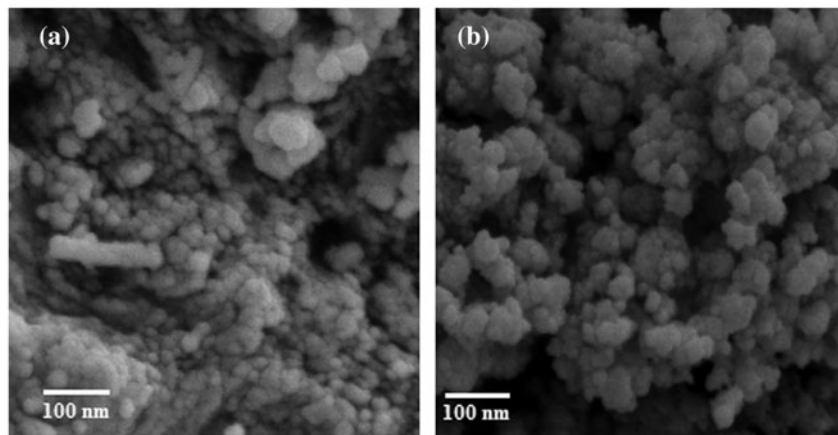


Fig. 2. The SEM image of calcined alunite (a) and magnetic alunite (b).

maximum sorption of both ions was obtained at pH of 6.0–10.0. By increasing pH, concentration of  $H^+$  ions gets decreased. Consequently, the competition between  $H^+$  and cations of heavy metals was reduced. At high pH (>7.0), the metal ions could precipitate as hydroxide form, which leads to the decrease in recovery. Therefore, a pH value of 6–7 was found to be an optimum pH for the simultaneous determination of Cu and Pb.

### 3.3. Effect of adsorbent dosage

In order to study the effects of amount of adsorbent on sorption of metal ions at optimum pH, different dosages of magnetic nanocomposite from 10 to 50 mg were tested according to general procedure for the adsorption of Cu(II) and Pb(II). The results showed (Fig. 3(b)) that adsorption percentage increased rapidly by increasing the adsorbent dosage

up to 30 mg due to the higher number of adsorption sites. However, a further increase from 30 to 50 mg did not make any changes in adsorption percentage of analytes. Excess amount of adsorbent is not economical as well as requiring larger elution volume. Therefore, the optimum amount of adsorbent was chosen to be 30 mg and further extraction experiments were carried out with the same.

### 3.4. Effect of extraction time

Extraction time is an important factor in SPE since for the complete quantitative extraction of metal ions by batch method, time should be long enough for interaction between liquid and solid phase. However, too long extraction time is useful, and also, for efficient preconcentration, it must be short enough. At the same time, too short time results in incomplete extraction [23,24]. Thus, in order to determine the optimum

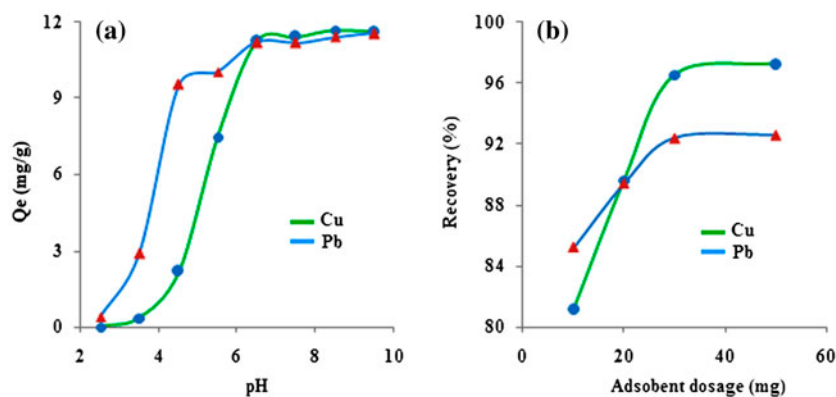


Fig. 3. Effect of pH (a) and adsorbent dosage (b) on copper and lead adsorption.

extraction time, sorption of Cu(II) and Pb(II) on magnetic nanocomposite has been investigated with shaking times of 2–15 min. Model solutions consisting 50 mL of 5 mg L<sup>-1</sup> of metal ions were used.  $Q_e$  increased rapidly in the first 10 min. This high initial uptake rate could be due to the availability of a large number of adsorption sites. Afterward, the increase in  $q_e$  was not significant as the sites are gradually filled up. Hence, a time of 10 min was selected for further experiments as an optimal time.

### 3.5. Selection of eluent

Selection of a proper eluent is a mainstay part of extraction since its type, volume, and concentration could affect the preconcentration process [25]. Thus, some experiments were carried out with the aim of choosing the most effective eluent for the quantitative desorption of adsorbed ions. As the adsorption of the analytes was negligible at acidic pH, desorption of metal ions was achieved at low pH. Various acidic solutions such as nitric acid, hydrochloric acid, and their combination were tested as eluents. HCl was suitable for desorption of Pb(II) but complete elution was not achieved for Cu(II). Among different cases, HNO<sub>3</sub> desorbed both ions better than other tested solutions and it was found that 5 mL of 0.5 mol L<sup>-1</sup> HNO<sub>3</sub> was sufficient for complete elution with a shaking time of 5 min. Hence, the recovery of 99.7 and 100% was achieved with 5 mL of eluent for Cu(II) and Pb(II), respectively.

### 3.6. Kinetic models

Several kinetic models are available to examine the controlling mechanism of the adsorption process and to test the experimental data. Kinetic measurements were made under the optimum conditions by batch extraction at different times. Five of the main kinetic models proposed in the literature were applied to the experimental data to determine the kinetic parameters and investigate the mechanism of adsorption of lead and copper by magnetic MnFe<sub>2</sub>O<sub>4</sub>@calcined alunite as an adsorbent. The rate of the adsorptive interactions can be evaluated using the linear form of integrating the Lagergren pseudo-first-order equation (Eq. (2)) which is the most widely used procedure for the adsorption of solute from aqueous solution under the boundary condition,  $t = 0$  to  $t = t$  and  $Q_t = 0$  to  $Q_t = Q_t$ .

$$\ln(Q_e - Q_t) = \ln Q_e - k_1 t \quad (2)$$

where  $k_1$  is the pseudo-first-order adsorption rate constant and  $Q_e$ ,  $Q_t$  are the values of the amount adsorbed per unit mass at equilibrium and at any time  $t$  (mg g<sup>-1</sup>). The values of  $Q_e$  and  $k_1$  (mg g<sup>-1</sup> min<sup>-1</sup>) can be determined experimentally by plotting the linear form of first-order model,  $\ln(Q_e - Q_t)$  vs.  $t$  [26,27], for both metal ions (Fig. 4(a) and (b)).

Pseudo-second-order kinetics is based on the adsorption capacity of solid sorbent. Furthermore, it is in agreement with chemisorption being the rate-controlling step and expressed as:

$$t/Q_t = 1/k_2 Q_e^2 + t/Q_e \quad (3)$$

where  $k_2$  (mg/g min) is the pseudo-second-order rate constant of adsorption [28]. The equilibrium adsorption capacity ( $Q_e$ ) and  $k_2$  can be found experimentally from the slope and intercept of plot  $t/Q_t$  vs.  $t$  (Fig. 4(c) and (d)).

The possibility of diffusion was explored using the intraparticle diffusion model (Eq. (4)). If the diffusion of metal ions on internal surfaces of pores and capillaries of the adsorbent is the rate-limiting step, the adsorption can be presented by the following equation:

$$Q_t = k_p t^{1/2} + C \quad (4)$$

where  $k_p$  represents intraparticle diffusion rate constant and  $C$  is a constant (mg g<sup>-1</sup>) which gives information about the thickness of boundary layer [29]. The plot of  $Q_t$  against  $t^{1/2}$  yields a straight line passing through the origin in case of intraparticle diffusion (Fig. 5(a) and (b)).

The liquid film diffusion model (Eq. (5)), which explains the role of transport of the adsorbate from the liquid-phase up to the solid-phase boundary, can be expressed as:

$$\ln(1 - F) = -k_{fd} t \quad (5)$$

where  $F$  is the fractional attainment of equilibrium ( $F = Q_t/Q_e$ ) and  $k_{fd}$  is the adsorption rate constant. A linear plot of  $-\ln(1 - F)$  vs.  $t$  (Fig. 5(c) and (d)) with zero intercept would suggest that the kinetics of sorption process is controlled by diffusion through the liquid film surrounding the solid sorbents.

As the results indicate in Table 1, experimental data gave poor fits with pseudo-first-order since the correlation coefficients were 0.97 and 0.85, respectively, and there was a difference between the experimental  $Q_e$  value and that obtained from the Lagergren

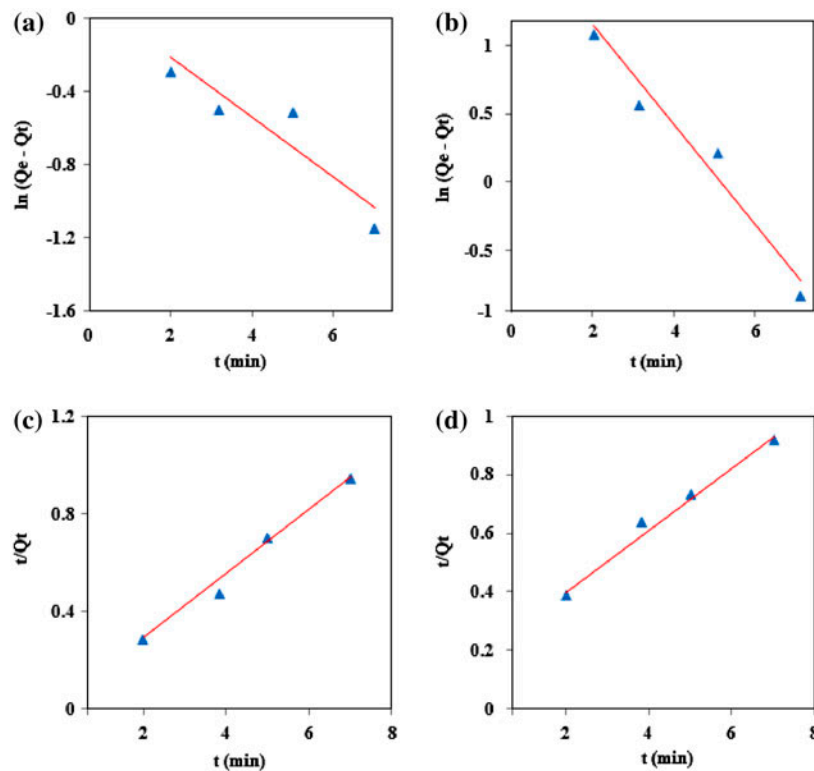


Fig. 4. First-order (a,b) and second-order plots (c,d) for lead and copper adsorption, respectively.

plot for both metal ions. The correlation coefficients obtained from pseudo-second-order model were found to be higher than 0.99 for both investigated analytes. Also, the theoretical  $Q_e$  of both ions was close to their experimental values; thus, this model could be the best for describing the kinetics of adsorption of copper and lead ions.

The existence of other process such as intraparticle diffusion was also investigated. Experimental data of  $Pb^{2+}$  did not fit to this model as correlation coefficient was not high enough. In contrast, the high linearity of the intraparticle diffusion plot for the adsorption of  $Cu^{2+}$  indicated that the intraparticle diffusion occurred. The line did not pass through an origin; thus, it was not the only rate-limiting parameter.

The film diffusion curve for  $Cu^{2+}$  exhibited linear plots with a correlation coefficient value of 0.97 and non-zero intercept (0.1813); this proved the role of film diffusion in the adsorption of  $Cu^{2+}$ , although the non-zero intercept limited applicability of this model. The film diffusion plot for Pb was not linear with a correlation coefficient of 0.85. Thus, this model could not describe the adsorption of  $Pb^{2+}$  on magnetic nanocomposite.

### 3.7. Adsorption isotherms

Developing an appropriate isotherm model for adsorption is essential for the design and optimization of adsorption processes. In this study, the equilibrium data were analyzed in accordance with the Langmuir and Freundlich isotherms. Langmuir model, which is based on the assumption that adsorption occurs at specific homogeneous monolayer surface containing finite number of identical sites, is one of the most common models used to investigate the adsorption isotherms [30–32]. The linear form of Langmuir isotherm model (Eq. (6)) can be written as follows:

$$C_e/Q_e = C_e/Q_m + 1/Q_m K_a \quad (6)$$

where  $C_e$  is the equilibrium concentration ( $mg L^{-1}$ ),  $Q_e$  is the amount of adsorbed ions at equilibrium ( $mg g^{-1}$ ),  $Q_m$  is the maximum adsorption capacity of a monolayer ( $mg g^{-1}$ ), and  $K_a$  is the energy of adsorption (Langmuir constant,  $L g^{-1}$ ). The values of  $Q_m$  and  $K_a$  were calculated from the slope and intercept of  $C_e/Q_e$  vs.  $C_e$  (Fig. 6(a) and (b)).

Another common isotherm model is Freundlich isotherm which describes that adsorption occurs on a

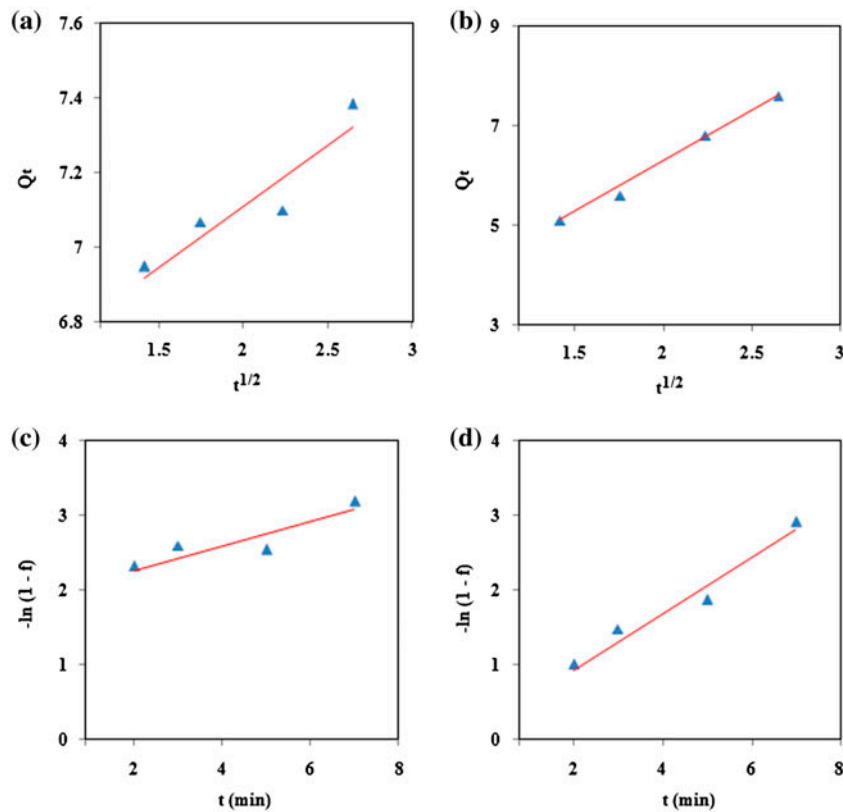


Fig. 5. Intraparticle diffusion (a,b) and liquid film diffusion (c,d) model of lead and copper adsorption.

Table 1  
Parameters of adsorption of  $\text{Cu}^{2+}$  and  $\text{Pb}^{2+}$  onto manganese ferrite@alunite nanocomposite

Ion	Pseudo-first-order			Pseudo-second-order			Intraparticle diffusion			Film liquid diffusion
	$Q_e$	$R^2$	$K_1$	$Q_e$	$R^2$	$K_2$	$K_p$	$C$	$R^2$	$R^2$
$\text{Cu}^{2+}$	6.66	0.97	0.375	9.5	0.99	0.056	2.034	2.23	0.99	0.97
$\text{Pb}^{2+}$	1.12	0.85	0.164	7.5	0.99	0.063	2.327	6.45	0.87	0.85

heterogeneous surface and hence does not assume monolayer capacity. The adsorption occurs at sites with different energies and the energy of adsorption varies as a function of surface coverage [33]. The linear form of Freundlich isotherm (Eq. (7)) is expressed as:

$$\log Q_e = \log K_f + 1/n \log C_e \tag{7}$$

where  $K_f$  and  $n$  are calculated from the intercept and slope of the linear plot of  $\log Q_e$  vs.  $\log C_e$  (Fig. 6(c) and (d)). The magnitude of the Freundlich constant ( $n$ ) gives a measure of favorability of adsorption as the values between 1 and 10 represent a favorable sorp-

tion. The values of Langmuir and Freundlich constants and the correlation coefficients for adsorption of  $\text{Cu}^{2+}$  and  $\text{Pb}^{2+}$  on magnetic alunite nanocomposite are summarized in Table 2. As it can be seen, experimental data fit well with both models as values of the correlation coefficient ( $R^2$ ) are close to 1. It indicates that both monolayer adsorption and heterogeneous energetic distribution of active sites on the surface of the adsorbent are possible. Moreover, adsorption mechanism for SPE of ions on manganese ferrite@alunite nanocomposite could be both ion exchange and complexation, since Langmuir isotherm proves the ion exchange mechanism and Freundlich isotherm represents the complexation mechanism [34,35]. Table 2

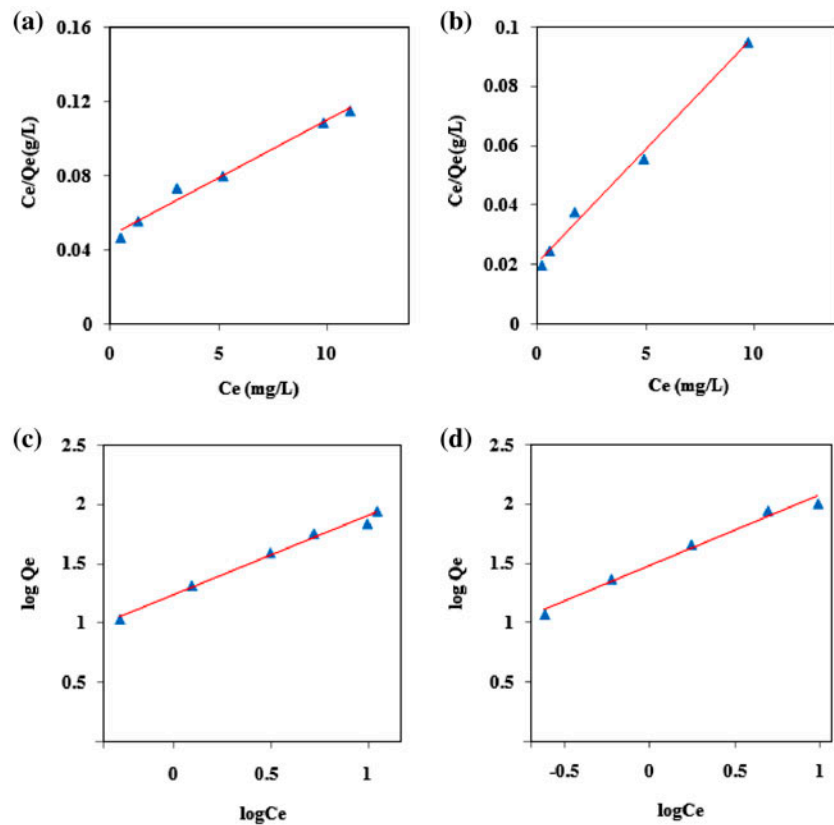


Fig. 6. Langmuir (a,b) and Freundlich isotherm (c,d) models for lead and copper adsorption.

Table 2

Langmuir and Freundlich parameters for the adsorption of  $\text{Cu}^{2+}$  and  $\text{Pb}^{2+}$  onto manganese ferrite@alunite nanocomposite

Ion	Freundlich isotherm			Langmuir isotherm		
	$K_f$ ( $\text{mg}^{1-1/n} \text{L}^{1/n} \text{g}^{-1}$ )	$n$ ( $\text{L mg}^{-1}$ )	$R^2$	$Q_m$ ( $\text{mg g}^{-1}$ )	$K_a$ ( $\text{L mg}^{-1}$ )	$R^2$
$\text{Cu}^{2+}$	28.84	1.7280	0.989	129.87	2.6635	0.9932
$\text{Pb}^{2+}$	18.5652	1.4749	0.9888	158.73	7.53	0.984

indicates that  $Q_m$  values of manganese ferrite@alunite nanocomposite for adsorption of  $\text{Cu}^{2+}$  and  $\text{Pb}^{2+}$  are 129.87 and 158.73  $\text{mg g}^{-1}$ , respectively. Also, value of Freundlich constant ( $n$ ) indicates that sorption process is favorable.

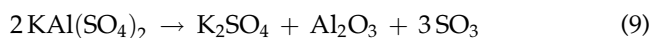
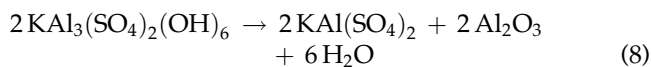
### 3.8. Adsorption mechanism

Heavy metal adsorption onto the magnetic composite may take place through physical or chemical adsorption. The results of kinetic and isotherm studies exhibited a standpoint about the adsorption mechanism. Second-order model is equal to chemisorption; however, first-order kinetic model represents physical

adsorption or ion exchange mechanism. Moreover, Freundlich isotherm corresponds to multilayer physical adsorption, while the Langmuir model shows monolayer chemisorption process. According to the experimental results, lead and copper sorption is along with a physicochemical sorption process, because the adsorption followed second-order kinetic model, as well as adsorption isotherm goodly fitted with both Langmuir and Freundlich model. This result indicates that the mechanism of lead and copper adsorption is complex and both the chemical and physical adsorptions exist at the same time in this adsorption process.

More perception of lead and copper adsorption mechanism can be obtained by describing the

structure of the adsorbent. During calcination stage of alunite at the temperature lower than 700 °C, the loss of water and formation of aluminum sulfate and  $\gamma$ -Al<sub>2</sub>O<sub>3</sub> were occurred. This process can be explained by the Eqs. (8) and (9):



In brief, calcined alunite contains Al<sub>2</sub>O<sub>3</sub> as the main component. After preparing nanocomposite, two oxide species, i.e. Fe<sub>2</sub>O<sub>3</sub> and MnO, superimposed to the alumina structure. In other words, the adsorbent composed from mixed oxides and the hydroxyl groups are the main functional groups on their structure. As a result, the mechanism for divalent copper and lead adsorption onto the composite can be expressed as follows (Eqs. (10)–(12)):



where S and M correspond to sorbent and the target ions (Pb<sup>2+</sup> and Cu<sup>2+</sup>), respectively. Eq. (10) represents ion exchange of hydrolyzed divalent metal cation (MOH<sup>+</sup>) in aqueous solution and H<sup>+</sup> in the sorbent structure. Electrostatic interaction (Eq. (11)) is another mechanism. Formation of inner and outer sphere complexes on the composite surface with S–O group is another main mechanism (Eq. (12)). However, the experimental results (kinetic and isotherm study) sustained complex formation (chemisorption) as the main adsorption mechanism.

### 3.9. Specificity of the sorbent

Specificity of the nanocomposite toward copper and lead is an another issue which has been confirmed based on the experimental results. As can be seen in Fig. 1(a), the sorbent showed higher efficiency for copper and lead uptake relative to other ions. This can be owing to the strong interaction between the target analytes and the sorbent functional groups. In other words, specific adsorption or overlapping between bonding orbitals of the species is involved in the reaction as the metal–sorbent considered to form a rigid complex in which their structure does not

change in the course of charge transfer. Another factor that seems to be premier relative to the above description, is the match between the radius of the metal ions and the size of pore structure on the surface of the nanocomposite. As a result, lead and copper ions can be separated in a relatively specific way from complicated matrices.

### 3.10. Effect of sample volume

In preconcentration step, for effectively enriching low concentration of analytes, high preconcentration factor is required. A higher preconcentration factor can be obtained by increasing the sample to eluent volume ratio. Effect of sample volumes from 50 to 500 mL containing 5 µg of Cu(II) and Pb(II) was studied under the optimum conditions. Results indicated that Cu(II) and Pb(II) ions were quantitatively recovered when the sample volumes were less than 400 and 300 mL as after elution with 5 mL of the eluent, an enrichment factor of 80 and 60 was achieved for Cu(II) and Pb(II), respectively.

### 3.11. Interferences

The effects of various common coexisting ions on the adsorption of copper and lead ions by the proposed method were investigated under the optimum conditions. Since the preconcentration of metal ions could be affected by the matrix constituents of samples. In these experiments, various salts and metal ions were added individually to the solutions of 100 µg L<sup>-1</sup> of Cu(II) and Pb(II) and treated according to the recommended procedure. The tolerance limit is defined as the ion concentration causing a relative error smaller than ±5% related to the preconcentration and determination of analytes. The results are shown in Table 3 and indicate that the procedure has good tolerance limit for adsorption of lead and copper from complex matrix.

### 3.12. Figures of merits

Under optimized conditions, calibration curves were constructed for Cu(II) and Pb(II) with the correlation factor of 0.9928 ( $A = 1.3791 C + 0.0066$ ) and 0.9937 ( $A = 0.5769 C - 0.0038$ ), respectively. Linearity in the final solution was maintained at 0.005–0.150 mg L<sup>-1</sup> for lead and 0.004–0.150 mg L<sup>-1</sup> for copper. The detection limits were calculated as three times the standard deviation of the blank signal ( $n = 8$ ) with preconcentration step and they were 0.69 and 0.91 µg L<sup>-1</sup>, for Pb(II)

Table 3

Effect of interfering ions on adsorption of Cu<sup>2+</sup> and Pb<sup>2+</sup> onto manganese ferrite@alunite nanocomposite

Ion	Ratio ion/Cu	Recovery (%)	Ratio ion/Pb	Recovery (%)
Na <sup>+</sup>	400	96 ± 1.1	5,000	101 ± 1.6
K <sup>+</sup>	5,000	98 ± 1.1	5,000	99.4 ± 1.9
Mg <sup>2+</sup>	1,000	95 ± 1.4	5,000	100 ± 1.5
NO <sub>3</sub> <sup>-</sup>	500	96 ± 1.3	500	98 ± 1.8
Zn <sup>2+</sup>	500	98.2 ± 1.6	500	98.9 ± 1.5
Co <sup>2+</sup>	500	99 ± 1.6	500	99.6 ± 1.2
Ni <sup>2+</sup>	500	97.5 ± 1.5	500	98.2 ± 1.4
Cr <sup>3+</sup>	300	96 ± 1.3	500	98 ± 1.8
Cd <sup>2+</sup>	500	96.2 ± 1.7	500	100.2 ± 1.7
Mn <sup>2+</sup>	500	95 ± 1.2	500	99 ± 1.5
HPO <sub>4</sub> <sup>2-</sup>	400	96 ± 1.1	5,000	101 ± 1.6
Cl <sup>-</sup>	5,000	98 ± 1.1	5,000	99.4 ± 1.9

Table 4

Analytical results for the determination of Cu<sup>2+</sup> and Pb<sup>2+</sup> in real samples

Sample	Added Cu (µg L <sup>-1</sup> )	Found Cu (µg L <sup>-1</sup> )	Recovery (%)	Added Pb (µg L <sup>-1</sup> )	Found Pb (µg L <sup>-1</sup> )	Recovery (%)
Mushroom	–	26.8	–	–	38	–
	100	123	97	100	133	96.3
Sausage	–	17	–	–	23	–
	100	112	95.72	100	119.3	99.6
Tomato	–	14.7	–	–	26	–
	100	111	96.8	100	124	98.4
Sea water	–	13.5	–	–	150	–
	100	3/112	98.9	100	241	96.4

and Cu(II), respectively. The procedure was repeated six times for determination of 100 µg L<sup>-1</sup> of ions and the relative standard deviation (RSD) was found to be 3.46% for Pb<sup>2+</sup> and 2.01% for Cu<sup>2+</sup>.

### 3.13. Application to real samples

In order to investigate the applicability of proposed method, determination of lead and copper ions in natural water and acid-digested samples was per-

formed. The results are presented in Table 4 and show that the recovery was in the range of 96–99%. Hence, the method has good efficiency to preconcentration of heavy metals from real samples.

### 3.14. Comparison with other methods

A comparison of proposed SPE method using manganese ferrite@ alunite nanocomposite with other types of sorbents which have been reported previously

Table 5

Comparison of the proposed method with some recent studies for simultaneous preconcentration of copper and lead

Ions	Adsorbent	Method	PF	LOD (µL <sup>-1</sup> )	RSD (%)	Q <sub>m</sub> (mg g <sup>-1</sup> )	Sample type	Refs.
Pb	Alumina	FAAS	250	0.17	3.2	16.4	Lettuce, water	[21]
Cu, Pb	Nano-TiO <sub>2</sub>	FAAS	83.3	0.15, 1.38	4.63, 4.83	3.95, 3.17	Water, Ore	[22]
Cu, Pb	Oxidized SWCNT	ICP-MS	50	0.001, 0.039	3.9–5.2	5.4–6.2	Water	[23]
Cu	Soybean hull	FAAS	18	0.8	1.7	18	Food, water	[24]
Cu, Pb	Activated carbon	FAAS	100	0.2, 0.45	3.5, 1.9	78.2, 48.6	Water	[25]
Cu, Pb	This work	FAAS	80	0.91	1.01	129.87	Food, water	This work
			60	0.69	3.46	158.73		

for enrichment and determination of lead and copper is given in Table 5. As seen from the data, the proposed method has relatively higher adsorption capacity and lower LOD compared to other SPE-FAAS method; also, the performance of the method was good with respect to enrichment factor and applicability for real sample analysis; thus, the prepared sorbent is a good choice for separation and preconcentration of Cu and Pb ions prior to FAAS.

#### 4. Conclusion

In this work, manganese ferrite@alunite nanocomposite was synthesized through a convenient one-step coprecipitation method in which the formation of  $\text{MnFe}_2\text{O}_4$  nanoparticles and their bonds to the surface of calcined alunite was performed simultaneously. Moreover, the other main advantages of this synthesis method include simplicity, no requirements of using any cross-linking agents, cost effectiveness, and time-saving. The synthesized composite was then successfully applied as a new adsorbent for simultaneous enrichment as well as separation of trace amounts of copper and lead prior to their determination by FAAS. The effects of various parameters were studied; the optimum conditions were obtained and reported in detail. In comparison to some literature, the manganese ferrite@alunite nanocomposite had higher adsorption capacity and the adsorption of analytes was faster so much, so that it could be completed within 10 min. The SPE method also offered relatively high tolerance limit for interfering ions, good precision, and sensitivity, acceptable preconcentration factor, as well as good efficiency for preconcentration of these ions from real samples.

#### Acknowledgment

Support for this investigation by the Research Council of the University of Tehran through grants is gratefully acknowledged.

#### References

- [1] R.L. Frost, R.A. Wills, M.L. Weier, W. Martens, J.T. Kloprogge, A Raman spectroscopic study of alunites, *J. Mol. Struct.* 785 (2006) 123–132.
- [2] M. Özacar, I.A. Şengil, Adsorption of Acid Dyes from aqueous solutions by calcined alunite and granular activated carbon, *Adsorption* 8 (2002) 301–308.
- [3] M. Özacar, Adsorption of phosphate from aqueous solution onto Alunite, *Chemosphere* 51 (2003) 321–327.
- [4] M. Özacar, I.A. Şengil, Adsorption of Reactive Dyes on calcined alunite, *J. Hazard. Mater. B98* (2003) 211–224.
- [5] Q. Han, Z. Wang, J. Xia, S. Chen, X. Zhang, M. Ding, Facile and tunable fabrication of  $\text{Fe}_3\text{O}_4$ /Graphene oxide nanocomposite and their application in the magnetic solid-phase extraction of polycyclic aromatic hydrocarbons from environmental water samples, *Talanta* 101 (2012) 388–395.
- [6] Q. Gao, D. Luo, J. Ding, Y.Q. Feng, Rapid magnetic solid phase extraction based on magnetite/silica/poly (methacrylic acid-co-ethylene glycol dimethacrylate) composite microspheres for the determination of sulfonamide in milk samples, *J. Chromatogr. A* 1217 (2010) 5602–5609.
- [7] Y. Liu, H. Li, J.M. Lin, Magnetic solid phase extraction based on octadecyl functionalization of monodisperse magnetic ferrite microspheres for the determination of polycyclic aromatic hydrocarbons in aqueous samples coupled with gas chromatography-mass spectrometry, *Talanta* 77 (2009) 1037–1042.
- [8] K. Aguilar- Arteaga, J.A. Rodriguez, E. Barrado, Magnetic solids in analytical chemistry: A review, *Anal. Chim. Acta* 674 (2010) 157–165.
- [9] X. Zhang, H. Niu, Y. Pan, Y. Shi, Y. Cai, Chitosan-coated octadecyl-functionalized magnetite nanoparticles: Preparation and application in extraction of trace pollutants from environmental water samples, *Anal. Chem.* 82 (2010) 2363–2371.
- [10] L. Ai, H. Huang, Z. Chen, X. Wei, J. Jiang, Activated carbon/  $\text{CoFe}_2\text{O}_4$  composite: Facile synthesis, magnetic performance and their potential application for the removal of malachite green from water, *Chem. Eng. J.* 156 (2010) 243–249.
- [11] A. Mehdiinia, F. Roohi, A. Jabbari, Rapid magnetic solid phase extraction with *in situ* derivatization of methyl mercury in sea water by  $\text{Fe}_3\text{O}_4$ /polyaniline nanoparticle, *J. Chromatogr. A* 1218 (2011) 4269–4274.
- [12] S. Shafiu, R. Topkaya, A. Baykal, M.S. Toprak, Facile synthesis of PVA– $\text{MnFe}_2\text{O}_4$  nanocomposite: Its magnetic investigation, *Mater. Res. Bull.* 48 (2013) 4066–4071.
- [13] D. Chen, H.Y. Liu, L. Li, One-step synthesis of manganese ferrite nanoparticles by ultrasonic wave-assisted ball milling technology, *Mater. Chem. Phys.* 134 (2012) 921–924.
- [14] G. Giakisikli, A.N. Anthemidis, Magnetic materials as sorbents for metal/metalloid preconcentration and/or separation. A review, *Anal. Chim. Acta* 789 (2013) 1–16.
- [15] J.G. Parsons, M.L. Lopez, J.R. Peralta-Videa, J.L. Gardea-Torresdey, Determination of arsenic(III) and arsenic(V) binding to microwave assisted hydrothermal synthetically prepared  $\text{Fe}_3\text{O}_4$ ,  $\text{Mn}_3\text{O}_4$ , and  $\text{MnFe}_2\text{O}_4$  nanoadsorbents, *Microchem. J.* 91 (2009) 100–106.
- [16] L. Wang, J. Li, Y. Wang, L. Zhao, Q. Jiang, Adsorption capability for Congo red on nanocrystalline  $\text{MFe}_2\text{O}_4$  (M=Mn, Fe, Co, Ni) spinel ferrites, *Chem. Eng. J.* 181–182 (2012) 72–79.
- [17] S. Hashemian, M. Salimi, Nano composite a potential low cost adsorbent for removal of cyanine acid, *Chem. Eng. J.* 188 (2012) 57–63.

- [18] R. Bushra, M. Shahadat, A.S. Raeissi, S.A. Nabi, Development of nano composite adsorbent for removal of heavy metals from industrial effluent and synthetic mixtures; its conducting behavior, *Desalination* 289 (2012) 1–11.
- [19] A. Uzun, M. Soylak, L. Elçi, Preconcentration and separation with Amberlite XAD-4 resin; determination of Cu, Fe, Pb, Ni, Cd and Bi at trace levels in waste water samples by flame atomic absorption spectrometry, *Talanta* 54 (2001) 197–202.
- [20] W. Ngeontae, W. Aeungmaitrepirom, T. Tuntulani, Chemically modified silica gel with aminothioamidoanthraquinone for solid phase extraction and preconcentration of Pb(II), Cu(II), Ni(II), Co(II) and Cd (II), *Talanta* 71 (2007) 1075–1082.
- [21] M. Ezoddin, F. Shemirani, K. Abdi, M. Khosravi Saghezchi, M.R. Jamali, Application of modified nano-alumina as a solid phase extraction sorbent for the preconcentration of Cd and Pb in water and herbal samples prior to flame atomic absorption spectrometry determination, *J. Hazard. Mater.* 178 (2010) 900–905.
- [22] N. Pourreza, S. Rastegarzadeh, A. Larki, Simultaneous preconcentration of Cd(II), Cu(II) and Pb(II) on Nano-TiO<sub>2</sub> modified with 2-mercaptobenzothiazole prior to flame atomic absorption spectrometric determination, *J. Ind. Eng. Chem.s* 20 (2014) 2680–2686.
- [23] S. Chen, C. Liu, M. Yang, D. Lu, L. Zhu, Z. Wang, Solid-phase extraction of Cu, Co and Pb on oxidized single-walled carbon nanotubes and their determination by inductively coupled plasma mass spectrometry, *J. Hazard. Mater.* 170 (2009) 247–251.
- [24] G. Xiang, Y. Zhang, X. Jiang, L. He, L. Fan, W. Zhao, Determination of trace copper in food samples by flame atomic absorption spectrometry after solid phase extraction on modified soybean hull, *J. Hazard. Mater.* 179 (2010) 521–525.
- [25] C. Duran, D. Ozdes, H.T. Akcay, H. Serencam, M. Tufekci, Simultaneous separation and preconcentration of Cd(II), Co(II), and Ni(II) ions in environmental samples by carrier element-free coprecipitation method prior to their flame atomic absorption spectrometric determination, *Desalin. Water Treat.* 53 (2015) 390–397.
- [26] A. Khaled, A. El-Nemr, A. El-Sikaily, O. Abdelwahab, Treatment of artificial textile dye effluent containing Direct Yellow 12 by orange peel carbon, *Desalination* 238 (2009) 210–232.
- [27] N.K. Amin, Removal of direct blue-106 dye from aqueous solution using new activated carbons developed from pomegranate peel: Adsorption equilibrium and kinetics, *J. Hazard. Mater.* 165 (2009) 52–62.
- [28] H.Y. Zhu, R. Jiang, L. Xiao, W. Li, A novel magnetically separable  $\gamma$ -Fe<sub>2</sub>O<sub>3</sub>/crosslinked chitosan adsorbent: Preparation, characterization and adsorption application for removal of hazardous azo dye, *J. Hazard. Mater.* 179 (2010) 251–257.
- [29] R. Han, W. Zou, Z. Zhang, J. Shi, J. Yang, Removal of copper(II) and lead(II) from aqueous solution by manganese oxide coated sand, *J. Hazard. Mater.* 137 (2006) 384–395.
- [30] R.R. Sheha, A.A. El-Zahhar, Synthesis of some ferromagnetic composite resins and their metal removal characteristics in aqueous solutions, *J. Hazard. Mater.* 150 (2008) 795–803.
- [31] C. Er, B.F. Senkal, M. Yaman, Determination of lead in milk and yoghurt samples by solid phase extraction using a novel aminothiazole-polymeric resin, *Food Chem.* 137 (2013) 55–61.
- [32] K.Y. Foo, B.H. Hameed, Insights into the modeling of adsorption isotherm systems, *Chem. Eng. J.* 156 (2010) 2–10.
- [33] G. Limousin, J.P. Gaudet, L. Charlet, S. Szenknect, V. Barthès, M. Krimissa, Sorption isotherms: A review on physical bases, modeling and measurement, *Appl. Geochem.* 22 (2007) 249–275.
- [34] Y.S. Ho, Selection of optimum sorption isotherm, *Carbon* 42 (2004) 2115–2116.
- [35] H. Chen, A. Wang, Adsorption characteristics of Cu(II) from aqueous solution onto poly(acrylamide)/attapulgite composite, *J. Hazard. Mater.* 165 (2009) 223–231.